ISSN 1063-7710, Acoustical Physics, 2006, Vol. 52, No. 6, pp. 623–632. © Pleiades Publishing, Inc., 2006.
Published in Russian in Akusticheskiĭ Zhurnal, 2006, Vol. 52, No. 6, pp. 725–735.

Parabolic Equation for Nonlinear Acoustic Wave Propagation in Inhomogeneous Moving Media[1]

M. V. Aver'yanov[a], V. A. Khokhlova[a], O. A. Sapozhnikov[a], Ph. Blanc-Benon[b], and R. O. Cleveland[c]

[a] *Moscow State University, Vorob'evy gory, Moscow, 119992, Russia*
e-mail: vera@acs366.phys.msu.ru
[b] *LMFA, UMR CNRS 5509, Ecole Centrale de Lyon, 69134 Ecully Cedex, France*
e-mail: Philippe.Blanc-Benon@ec-lyon.fr
[c] *Department of Aerospace and Mechanical Engineering, Boston University, 110 Cummington Street, Boston, Massachusetts 02115, USA*
e-mail: robinc@bu.edu

Received October 10, 2005

Abstract—A new parabolic equation is derived to describe the propagation of nonlinear sound waves in inhomogeneous moving media. The equation accounts for diffraction, nonlinearity, absorption, scalar inhomogeneities (density and sound speed), and vectorial inhomogeneities (flow). A numerical algorithm employed earlier to solve the KZK equation is adapted to this more general case. A two-dimensional version of the algorithm is used to investigate the propagation of nonlinear periodic waves in media with random inhomogeneities. For the case of scalar inhomogeneities, including the case of a flow parallel to the wave propagation direction, a complex acoustic field structure with multiple caustics is obtained. Inclusion of the transverse component of vectorial random inhomogeneities has little effect on the acoustic field. However, when a uniform transverse flow is present, the field structure is shifted without changing its morphology. The impact of nonlinearity is twofold: it produces strong shock waves in focal regions, while, outside the caustics, it produces higher harmonics without any shocks. When the intensity is averaged across the beam propagating through a random medium, it evolves similarly to the intensity of a plane nonlinear wave, indicating that the transverse redistribution of acoustic energy gives no considerable contribution to nonlinear absorption.

PACS numbers: 43.25.Jh, 43.28.Gq

DOI: 10.1134/S1063771006060017

1. INTRODUCTION

Nonlinear propagation of intense acoustic waves through an inhomogeneous moving medium has many diverse applications, for example, the propagation of sonic booms through the turbulent boundary layer near the ground [1, 2], the propagation of shock waves from explosive sources in the ocean [3, 4], and the propagation of high-intensity ultrasound and shock waves in inhomogeneous tissue with blood flow [5]. In these applications, the determination of the acoustic field has important ramifications, for example, prediction of the loudness of sonic booms or assessment of ultrasound-induced bioeffects in tissue. It is desirable to be able to predict average values of the pressure field, as well as peak values. This requires a model that accounts for the effects of inhomogeneities, diffraction, nonlinearity and absorption.

Inhomogeneities can be classified into two types: scalar inhomogeneities, that is, spatial fluctuations of sound speed and density, for example, due to variations in temperature or salt concentration in the ocean or variations in tissue type, and vector inhomogeneities, that is, spatial fluctuations of the background particle velocity, for example, due to the presence of vortices, wind, or flow in the medium. A complete theoretical model that incorporates the vectorial type of inhomogeneities is very complicated for analysis. A common approach is to replace the real moving medium with a hypothetical motionless medium with an effective sound speed that takes into account only the velocity component along the direction of propagation; that is, the moving medium is modeled as a medium with scalar-type inhomogeneities. A detailed analysis of this approach can be found in [6]. However, in many problems, refracted sound waves and those scattered by inhomogeneities propagate in directions that may considerably differ from the initial one. Furthermore, if the transverse component of the velocity field has a nonzero mean component, this may also result in a shift and distortion of the caustics and, therefore, may have a strong effect on further propagation of the acoustic wave.

[1] This article was translated by the authors.

Most results for vectorial-type inhomogeneities had been obtained for simplified models, generally under the assumption of nonlinear geometrical acoustics [7]. However, even in this case, analytical solutions had been obtained only for stratified media [7, 8]. Recently, parabolic equations were derived for linear sound propagation in inhomogeneous moving media [9–11], which retain the vector properties of the velocity of the medium. Nonlinear propagation in media with scalar inhomogeneities was also considered in the parabolic approximation [12–15]. To the best of our knowledge, nonlinear propagation of diffracted sound beams in random inhomogeneous moving media has never been investigated.

In this work, a nonlinear parabolic wave equation that accounts for both scalar and vector inhomogeneities of a medium is derived. A frequency-domain numerical algorithm is developed to model the nonlinear propagation of periodic signals in randomly inhomogeneous media. Numerical simulations are used to determine the influence of nonlinearity, diffraction, and scalar and vector inhomogeneities on the initially plane harmonic wave propagation in a random medium.

2. THEORETICAL MODEL

A rigorous way to incorporate the effects of the velocity field is to begin with the fundamental equations of fluid mechanics and derive a wave equation that accounts for fluctuations in the sound speed, density, and all the components of the velocity of the moving medium. This has been done for the case of linear waves [2, 4, 6]; the equation that describes acoustic wave propagation through scalar and vector-type inhomogeneities is as follows:

$$\frac{d}{dt}\frac{\partial}{\partial t}\left(\frac{1}{\rho c^2}\frac{dp}{dt}\right) - \vec{\nabla}\frac{\partial}{\partial t}\left(\frac{\vec{\nabla}p}{\rho}\right) + 2\frac{\partial u_i}{\partial x_j}\frac{\partial}{\partial x_i}\left(\frac{1}{\rho}\frac{\partial p}{\partial x_j}\right) = 0. \quad (1)$$

Here, p is the acoustic pressure, x_i ($i = 1, 2, 3$) are the components of the position vector $\vec{r}$ in Cartesian coordinates, c is the speed of sound; ρ is the density; t is the time, and u_i are the components of the velocity of the medium (which we will refer to as the flow) along the x, y, and z coordinate axes. The variables p, c, ρ, $\vec{u}$ are functions of time t and x, y, z coordinates; $d/dt = \partial/\partial t + (\vec{u}\cdot\vec{\nabla})$. Beyond the usual paradigm of linear lossless acoustics, the only restriction on the use of this equation is that the Mach number associated with the flow be small: $|\vec{u}|/c_0 \ll 1$, where c_0 is the ambient sound speed.

In this paper, the method of slowly varying amplitude [16] is used to reduce Eq. (1) to a linear parabolic equation. According to this method, the solution is represented in the form $p = p$, where $\tau = t - z/c_0$, $X = \varepsilon x$, $Y = \sqrt{\varepsilon}\,y$, $Z = \sqrt{\varepsilon}\,z$, τ is the retarded time and ε is a small parameter. In this representation, the direction of the cartesian x axis is the initial direction of wave propagation. The derivatives in Eq. (1) are transformed as follows:

$$\begin{gathered}\partial/\partial t \longrightarrow \partial/\partial\tau, \quad \partial^2/\partial t^2 \longrightarrow \partial^2/\partial\tau^2,\\ \partial/\partial x \longrightarrow -1/c_0\partial/\partial\tau + \varepsilon\partial/\partial X,\\ \partial^2/\partial x^2 \longrightarrow 1/c_0^2\partial^2/\partial\tau^2 - 2\varepsilon/c_0\partial^2/\partial X\partial\tau + \varepsilon^2\partial^2/\partial X^2,\\ \partial/\partial y \longrightarrow \sqrt{\varepsilon}\partial/\partial Y, \quad \partial^2/\partial y^2 \longrightarrow \varepsilon\partial^2/\partial Y^2,\\ \partial/\partial z \longrightarrow \sqrt{\varepsilon}\partial/\partial Z, \quad \partial^2/\partial z^2 \longrightarrow \varepsilon\partial^2/\partial Z^2.\end{gathered} \quad (2)$$

Substituting relations (2) into Eq. (1), neglecting the terms on the order of ε^2 in the stretched coordinate system (X, Y, Z), and returning to the original (x, y, z) coordinates, we obtain

$$\begin{aligned}&\overset{1}{\left[\frac{2}{c_0}\frac{\partial^2}{\partial x\partial\tau}\right.} \overset{2}{-\Delta_\perp} + \overset{3}{\left(\frac{1}{c^2}-\frac{1}{c_0^2}\right)\frac{\partial^2}{\partial\tau^2}} \overset{4}{-\frac{2u_x}{c^2c_0}\frac{\partial^2}{\partial\tau^2}}\\ &\overset{5}{+\frac{2}{c^2}(\vec{u}_\perp\vec{\nabla}_\perp)\frac{\partial}{\partial\tau}} + \overset{6}{\left(\frac{2}{c^2}u_x\frac{\partial}{\partial x}+\frac{2}{c_0^2}\frac{\partial u_x}{\partial x}\right)\frac{\partial}{\partial\tau}}\\ &\overset{7}{-\frac{1}{\rho c_0}\frac{\partial\rho}{\partial x}\frac{\partial}{\partial\tau}} \overset{8}{+\frac{1}{\rho}\vec{\nabla}_\perp\rho\cdot\vec{\nabla}_\perp} \overset{9}{-\frac{2}{c_0}\left(\vec{\nabla}_\perp u+\frac{\partial u_\perp}{\partial x}\right)\vec{\nabla}_\perp}\\ &\overset{10}{-\int\left(2\sum_{i=1}^{2}\sum_{j=1}^{2}\frac{\partial u_i}{\partial x_j}\frac{\partial^2}{\partial x_i\partial x_j}\right)d\tau} \overset{11}{+\frac{1}{\rho}\frac{\partial\rho}{\partial x}\frac{\partial}{\partial x}}\\ &\overset{12}{-\frac{4}{c_0}\frac{\partial u_x}{\partial x}\frac{\partial}{\partial x}} \overset{13}{+2\int\left(\frac{\partial\vec{u}_\perp}{\partial x}+\vec{\nabla}_\perp u_x\right)\frac{\partial}{\partial x}\vec{\nabla}_\perp d\tau}\left.\right]p = 0.\end{aligned} \quad (3)$$

Here, u_x is the longitudinal component of the flow in the medium, $\vec{u}_\perp = (u_y, u_z)$ represents the transverse components of the flow, and $\vec{\nabla}_\perp = (\partial/\partial y, \partial/\partial z)$. In the derivation of Eq. (3), it was assumed that all the inhomogeneities slowly vary in space, i.e., $\partial\rho/\partial X_i$, $\partial c/\partial X_i$, and $\partial u_j/\partial X_i$ are on the order of ε. We also assume that the inhomogeneities known a priori are specified at the instants when the acoustic wave passes through them and remain unchanged during the passage of the acoustic wave. In this case, the sound speed, density, and velocity fields can be considered as functions of spatial coordinates alone: $c = c(x, y, z)$, $\rho = \rho(x, y, z)$, and $\vec{u} = \vec{u}(x, y, z)$; i.e., they are "frozen" in time. Equation (3) is the most complete linear parabolic equation that

describes the propagation of sound waves in inhomogeneous moving media. For harmonic waves, it can be reduced to the form identical with the equation derived by Ostashev with the same enumeration of terms [2].

Equation (3) is still rather complicated for numerical modeling. Actually, it contains six physical parameters assumed to be of the same order of smallness. These parameters are as follows: $1/kL$, where L is the characteristic scale of inhomogeneity and k is the acoustic wave number; the acoustic Mach number $p/c_0^2\rho_0$; the flow Mach number $|\vec{u}|/c_0$; $\Delta c/c_0 = (c - c_0)/c_0$ is the parameter associated with scalar inhomogeneities of the sound speed; $\Delta\rho/\rho_0$ is the parameter associated with variations in density; and the angle between the direction of wave propagation and the x axis. Following the arguments by Ostashev [2], we retain only terms with numbers 1–5, which are on the order of $1/kL$, and neglect the terms containing combinations of any aforementioned small parameters. In addition, we keep the term of number 7 related to density variations, because, in the absence of any sound speed fluctuations or medium flow, this term becomes the most significant one. The resulting linear parabolic wave equation is

$$\frac{\partial}{\partial\tau}\left[\frac{\partial p}{\partial x} - \frac{\Delta c + u_x}{c_0^2}\frac{\partial p}{\partial\tau} + \frac{1}{c_0}\vec{u}_\perp\vec{\nabla}_\perp p - \frac{p}{2\rho}\frac{\partial\rho}{\partial x}\right] = \frac{c_0}{2}\Delta_\perp p, \quad (4)$$

which describes the acoustic wave propagation in a 3D inhomogeneous moving medium. In the absence of inhomogeneities, i.e., when Δc, $\Delta\rho$, and $\vec{u}$ are equal to zero, it is reduced to the well-known parabolic approximation of diffraction [16].

At the final step of the derivation of the nonlinear parabolic equation, we take into account that the terms describing nonlinearity and attenuation can be additively included into the linear parabolic equation [14, 16]. This can be justified on the grounds that the nonlinear and attenuation terms are small and, hence, any interaction with the other terms will necessarily be of higher order of smallness. Within the framework of our consideration, they can be neglected. Finally, we get the following nonlinear parabolic wave equation:

$$\frac{\partial}{\partial\tau}\left[\frac{\partial p}{\partial x} - \frac{\beta}{c_0^3\rho_0}p\frac{\partial p}{\partial\tau} - \frac{\Delta c + u_x}{c_0^2}\frac{\partial p}{\partial\tau} + \frac{1}{c_0}(\vec{u}_\perp\vec{\nabla}_\perp p) - \frac{p}{2\rho}\frac{\partial\rho}{\partial x} - \delta\frac{\partial^2 p}{\partial\tau^2}\right] = \frac{c_0}{2}\Delta_\perp p, \quad (5)$$

where β is the coefficient of nonlinearity and δ is the coefficient of the diffusivity of sound. The thermoviscous absorption term $\delta\partial^2 p/\partial\tau^2$ can be replaced by a more general linear operator $L(p)$ to account for relaxation or other losses [17].

Equation (5) is a KZK type of equation, which models the combined effects of diffraction, nonlinearity, and attenuation; it is generalized to account for sound speed and density inhomogeneities and flow inhomogeneities. In Eq. (5), the first term accounts for propagation, the second term for nonlinear distortion, the third for sound speed (scalar) and axial flow (vector) inhomogeneities, the fourth for transverse flow (vector) inhomogeneities, the fifth for density (scalar) inhomogeneities, and the sixth for absorption. The right-hand side accounts for effects of diffraction. What is new here is the addition of the fourth term associated with transverse flow effects.

In dimensionless coordinates and 2D Cartesian geometry, the modified KZK equation excluding scalar inhomogeneities can be represented as

$$\frac{\partial}{\partial\theta}\left[\frac{\partial V}{\partial\sigma} - NV\frac{\partial V}{\partial\theta} - 2\pi U_\parallel\frac{\partial V}{\partial\theta} + U_\perp\frac{\partial V}{\partial Y} - A\frac{\partial^2 V}{\partial\theta^2}\right] = \frac{1}{4\pi}\frac{\partial^2}{\partial Y^2}V. \quad (6)$$

Here, $V = p/p_0$ is the acoustic pressure normalized by its initial amplitude value; $\theta = \omega_0\tau$ is dimensionless time; $\omega_0 = 2\pi c_0/\lambda$ is the angular frequency; λ is the acoustic wavelength; $\sigma = x/\lambda$ is the normalized propagation distance; $Y = y/\lambda$ is the normalized transverse coordinate; $U_\parallel = u_x/c_0$ is the normalized axial flow; $U_\perp = u_y/c_0$ is the normalized transverse flow; $N = 2\pi\beta p_0/c_0^2\rho_0 = \lambda/x_p$ is a dimensionless nonlinear parameter, where $x_p = c_0^3\rho_0/\varepsilon p_0\omega_0$ is the shock formation distance for a harmonic plane wave; and $A = (2\pi)^2 c_0^2\delta/\lambda$ is a dimensionless parameter of absorption.

Equation (6) has no analytical solutions, but there exist some important properties of similarity, which can be used to obtain series of solutions to Eq. (6) if only one numerical solution is known. Generally, the motion of the medium can be represented as a mean motion with various fluctuations of velocity. Then, we can write the components of total velocity as $U_\parallel = U_\parallel^0 + \tilde{U}_\parallel$ and $U_\perp = U_\perp^0 + \tilde{U}_\perp$, where variables with a tilde represent velocity fluctuations and variables with zero index, the mean motion of the medium.

Let us consider a field of vectorial inhomogeneities with a mean motion governed by the laws $U_\parallel^0 = B(\sigma)Y + C(\sigma)$ and $U_\perp^0 = D(\sigma)$ and with arbitrary random fluctuations $\tilde{U}_\parallel$ and $\tilde{U}_\perp$. It can be shown that, using the transformation of variables

$$\theta_1 = \theta + \theta_{01}(\sigma) + \theta_{02}(\sigma)Y, \quad \sigma_1 = \sigma, \quad Y_1 = Y + Y_0(\sigma), \quad (7)$$

where the unknown functions $\theta_{01}(\sigma)$, $\theta_{02}(\sigma)$, and $Y_0(\sigma)$ can be obtained as the solutions to the system of differential equations

$$\frac{d\theta_{02}}{d\sigma} = 2\pi B, \quad \frac{d\theta_{01}}{d\sigma} = 2\pi C - D\theta_{02} + \frac{1}{4\pi}\theta_{02}^2, \qquad \frac{dY_0}{d\sigma} = -D + \frac{1}{2\pi}\theta_{02}, \tag{8}$$

it is possible to completely eliminate the mean motion of the medium from the parabolic equation while retaining the modified fluctuating components:

$$\frac{\partial}{\partial\theta_1}\left[\frac{\partial V}{\partial\sigma_1} - NV\frac{\partial V}{\partial\theta_1} - 2\pi\tilde{U}_\parallel^1\frac{\partial V}{\partial\theta_1} + \tilde{U}_\perp^1\frac{\partial V}{\partial Y_1} - A\frac{\partial^2 V}{\partial\theta_1^2}\right] = \frac{1}{4\pi}\frac{\partial^2}{\partial Y_1^2}V, \tag{9}$$

where

$$\tilde{U}_\parallel^1(\sigma_1, Y_1) \equiv \tilde{U}_\parallel(\sigma_1, Y_1 - Y_0(\sigma_1)) + \frac{1}{2\pi}\theta_{02}(\sigma_1)\tilde{U}_\perp(\sigma_1, Y_1 - Y_0(\sigma_1)), \qquad \tilde{U}_\perp^1(\sigma_1, Y_1) \equiv \tilde{U}_\perp(\sigma_1, Y_1 - Y_0(\sigma_1)). \tag{10}$$

Note that, according to Eqs. (10), fluctuations of the medium flow in the transverse direction influence the speed of sound of the wave. This can be interpreted physically as follows: as the phase front turns, the transverse flow is no longer perpendicular to the normal to the front, the flow projection onto the wave vector becomes nonzero, and, therefore, the transverse flow component causes a change in the phase velocity of the wave. In contrast, the projection of the longitudinal flow onto the normal to the steered wave vector does not manifest itself as a transverse flow. Presumably, this effect is a large-angle one, which is not taken into account by the parabolic approximation.

Consider an example of a layered inhomogeneous medium described by the law $U_\parallel^0 = B_0 Y + C_0$ and $U_\perp^0 = 0$, where B_0 and C_0 are arbitrary constants (horizontal flow with linearly varying amplitude in the transverse direction). This leads to the following change of variables:

$$\theta_1 = \theta - C_0\sigma + \frac{1}{12\pi}B_0^2\sigma^3 - B_0\sigma Y, \qquad \sigma_1 = \sigma, \quad Y_1 = Y - \frac{1}{4\pi}B_0\sigma^2. \tag{11}$$

From Eqs. (11), it can be deduced that the axis of the beam has a parabolic trajectory and the phase front turns due to the presence of flow. In the case of a purely transverse flow, i.e., when $U_\parallel^0 = 0$ and $U_\perp^0 = D(\sigma)$, the change of variables takes the form

$$\theta_1 = \theta, \quad \sigma_1 = \sigma, \quad Y_1 = Y - \int_0^\sigma D(\sigma')d\sigma'. \tag{12}$$

In this case, the axis of the sound beam has a trajectory governed by the function $D(\sigma)$, but the phase front does not turn. In geometrical acoustics, this leads to noncollinearity of phase and group velocities.

3. NUMERICAL ALGORITHM

Parabolic equations (5) and (6) are still sufficiently complicated for deep theoretical analysis and, therefore, need to be solved numerically. Depending on the temporal characteristics of the transmitted signal, different approaches can be employed for numerical modeling. The time-domain approach is more convenient for modeling the propagation of pulsed signals [12, 17], and the frequency-domain modeling (spectral approach) is better suited for describing periodic waves [15, 18].

To obtain the solution to Eq. (6), the spectral numerical algorithm presented in [18] for axially symmetric beams has been generalized to 2D Cartesian geometry. Representing the solution in the form of the Fourier series expansion [18] $V(\sigma, Y, \theta) = \sum_{n=-\infty}^{\infty} C_n(\sigma, Y)\exp(-in\theta)$ and substituting it into Eq. (6), we obtain a set of coupled nonlinear differential equations for the complex amplitudes C_n:

$$\frac{\partial C_n}{\partial\sigma} = \frac{i}{4\pi n}\frac{\partial^2}{\partial Y^2}C_n - \frac{in}{2}N\sum_{k=-\infty}^{\infty}C_k C_{n-k} - An^2 C_n - i2\pi n U_\parallel C_n - U_\perp\frac{\partial C_n}{\partial Y} = L_D + L_N + L_A + L_I, \tag{13}$$

where $C_n(\sigma, Y)$ is the complex amplitude of the nth harmonic ($-\infty < n < \infty$) and $C_{-n} = C_n^*$ (C_n^* denotes the complex conjugate of C_n).

Set of equations (13) is solved for the harmonic amplitudes C_n using a frequency-domain numerical algorithm based on the operator splitting procedure [18]. The amplitudes C_n of the first $n \le N_{\max}$ harmonics are calculated using a marching algorithm in the σ direction. At each step $\Delta\sigma$, the right-hand side of Eqs. (13) is split into four operators: L_D = diffraction, L_N = nonlinearity, L_A = absorption, and L_I = inhomogeneity. These operators are applied sequentially. At the first fractional step, the set of equations $\partial C_n/\partial\sigma = L_D$ is solved independently for each harmonic component n using a second-order Crank–Nicholson implicit algorithm. The results are then used as the boundary condition for the second fractional step, at which nonlinearity effects are included independently for each spatial grid point, $\partial C_n/\partial\sigma = L_N$, using a fourth-order Runge–Kutta algorithm. At the third fractional step, the absorption term, $\partial C_n/\partial\sigma = L_A$, is calculated by applying the exact solution $C_n(\sigma + \Delta\sigma) = C_n(\sigma)\exp(-An^2\Delta\sigma)$. The effects of inhomogeneities are taken into account at the last fractional step, $\partial C_n/\partial\sigma = L_I$, using the exact solu-

tion for the longitudinal component and a second-order Lax–Wendroff numerical algorithm for the transverse component of the velocity field [19].

In the simulations reported here, the value of the absorption coefficient A was chosen to provide the stability of the solution in accordance with the number of harmonics retained in the calculations and the maximum amplitude of the shock wave achieved. For a specific problem, the coefficient would be determined by the properties of the medium and the appropriate number of harmonics would have to be chosen for that case.

On the basis of the proposed numerical algorithm, we consider first the example of linear propagation of an initially plane harmonic wave through a singular focusing scalar Gaussian inhomogeneity of one-wavelength size: $U_{\parallel}^{0} = U\exp(-(\sigma - 10)^2 - Y^2)$ and $U_{\perp}^{0} = 0$ in Eq. (6). The value $U = 0.03$ was used, which resulted in a sound speed at the center of inhomogeneity about 3% lower than the background sound speed c_0 (Fig. 1a). This kind of inhomogeneity was chosen to compare the results with the solutions to the more precise wide-angle parabolic equation [10] and to the parabolic equation solved in the time domain [17] and, thus, to check the accuracy of the theoretical model and of the numerical scheme. During the propagation of the acoustic wave through the sound speed inhomogeneity, the initially plane wave front is distorted, resulting in the wave focusing and the formation of areas with increased pressure (Fig. 1b). The areas of defocusing and corresponding decrease in the pressure level are formed simultaneously with the focused regions. The amplitude of the wave along the axis passing through the center of the Gaussian inhomogeneity was found to be in good agreement with the solutions obtained on the basis of wide-angle parabolic approximation and using the time-domain parabolic model. The difference in the results was less than 3% when the spatial steps $\Delta\sigma$ and ΔY corresponded to 50 points per acoustic wavelength.

Then, a medium with flow inhomogeneities was modeled as a set of $J_{\max}$ randomly oriented Fourier modes (RFM) [20]:

$$\vec{u}(\vec{r}) = \sum_{j=1}^{J_{\max}} \vec{\tilde{U}}(\vec{K}_j)\cos(\vec{K}_j \cdot \vec{r} + \phi_j), \qquad (14)$$

$$\vec{\tilde{U}}(\vec{K}_j) \cdot \vec{K}_j = 0. \qquad (15)$$

Here, $\vec{K}_j$ is the mode wave vector and ϕ_j is the phase of the jth mode. The random angle θ_j between $\vec{K}_j$ and the x axis, as well as the phase ϕ_j for each Fourier component, were selected from independent uniform distributions within the interval $[0, 2\pi]$. Condition (15) is imposed to ensure that the resulting velocity field is incompressible. The velocity amplitude of each mode $|\vec{\tilde{U}}(\vec{K}_j)|$ in Eq. (14) is determined by the kinetic energy spectrum $E(K)$ of the particular turbulence model: $|\vec{\tilde{U}}(\vec{K}_j)| = \sqrt{E(K)}$, $K = |\vec{K}|$. In this paper, a spectrum derived from the longitudinal Gaussian correlation function $B_f(r) = \exp(-r^2/L^2)$ was used. In 2D Cartesian geometry, this correlation function corresponds to the spectrum

$$E(K) = \frac{1}{8}u_{rms}^2 K^3 L^4 \exp\left(-\frac{K^2L^2}{4}\right), \qquad (16)$$

where u_{rms}^2 is the mean square velocity fluctuation and L is the characteristic scale of the inhomogeneity. The

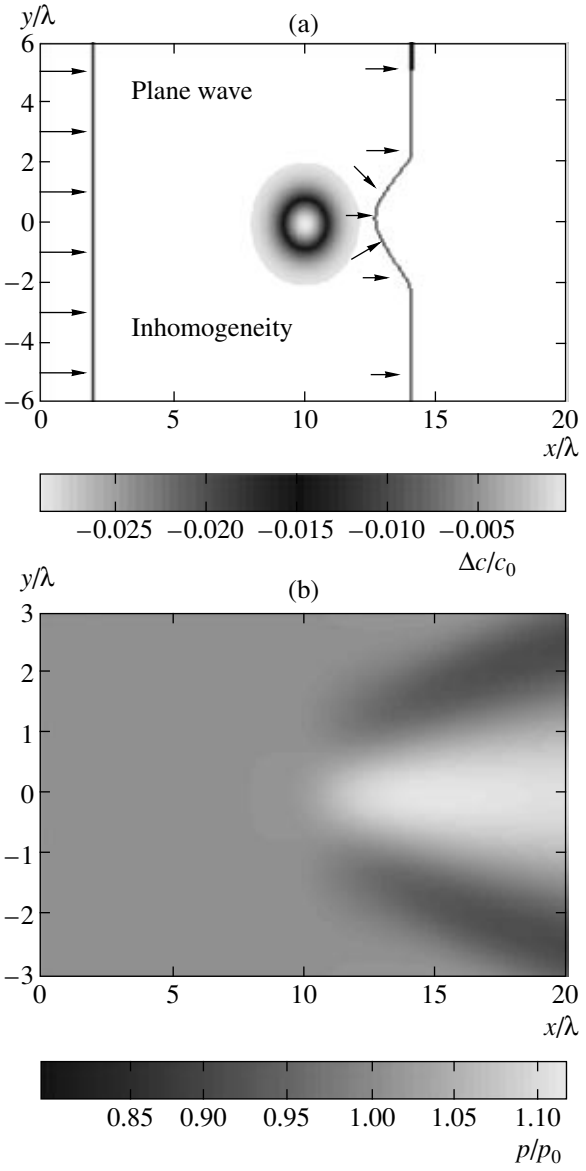

Fig. 1. (a) Sound speed map for a medium with a single scalar focusing Gaussian inhomogeneity with $\Delta c_{\max}/c_0 \sim 3\%$ and (b) the corresponding distribution of the peak acoustic pressure resulting from linear harmonic wave propagation through the inhomogeneity.

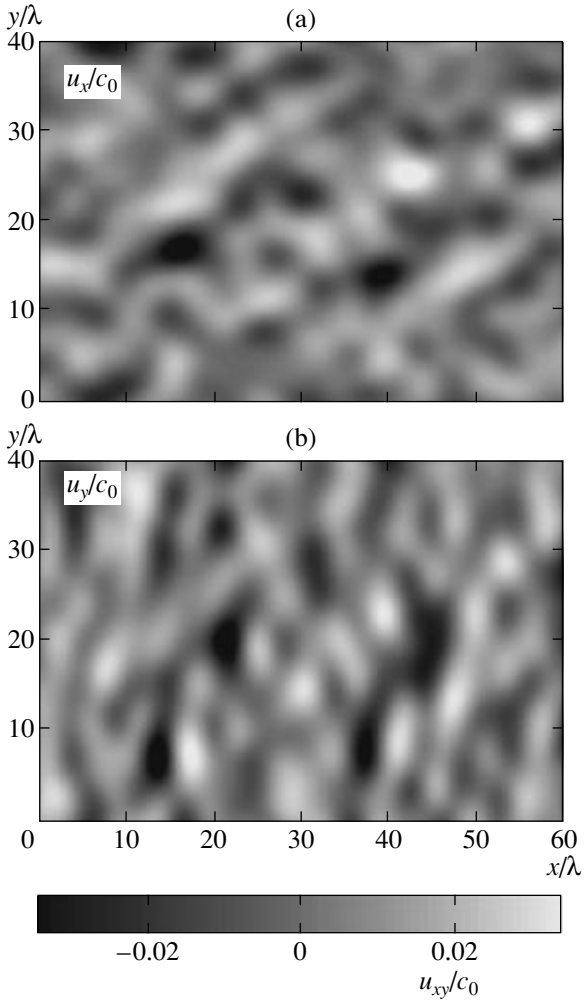

Fig. 2. (a) Longitudinal and (b) transverse components of the random velocity field used in this paper. The characteristic length of inhomogeneities is $L = 3\lambda$ and the maximum velocity fluctuations are $\max(u_x/c_0) = \max(u_y/c_0) = 0.03$.

longitudinal spatial correlation length L_f is equal to $L\sqrt{\pi}/2$. If a sufficiently large number of velocity modes in Eq. (14) are considered with each mode created according to Eq. (15) and with uniformly distributed θ_j and ϕ_j, the resulting velocity field $\vec{u}(\vec{r})$ is statistically homogeneous and isotropic with the prescribed energy spectrum [20]. In this paper, 300 Fourier modes equally spaced between $0.1/L$ and $10/L$ were used. Figure 2 shows the longitudinal $U_\parallel$ and transverse $U_\perp$ components of the random velocity field with the characteristic size of inhomogeneity structure $L = 3\lambda$ and with the amplitude $M = \max(U_\parallel, U_\perp) = 0.03$.

In modeling the acoustic field, the following parameters of the numerical scheme were used: $\Delta\sigma = 2.0 \times 10^{-3}$ and $\Delta Y = 2.5 \times 10^{-2}$ were the steps in longitudinal and transverse directions, respectively; $A = 0.002$ was the absorption parameter; and $N_{\max} = 150$ was the number of harmonics in the frequency spectrum. These parameters were chosen to provide the stability and sufficient accuracy of the algorithm. To avoid the reflections from the boundaries of the numerical domain, the spatial window in the transverse direction was chosen to be twice as large as the region of interest. In addition, according to the hypothesis of frozen turbulence, the random velocity field $\vec{u}(\vec{r})$ was considered to be constant in time.

4. RESULTS

Figure 3 shows the peak positive acoustic pressure patterns that correspond to the linear ($N = 0$) and nonlinear ($N = 0.05$) propagation of an initially plane harmonic wave through the random velocity field (Fig. 2). Both longitudinal and transverse components of the velocity were included in simulations. No absorption was applied in the case of linear propagation. Qualitatively, the morphology of the acoustic field could be predicted based on the data shown in Fig. 2; that is, regions of reduced effective sound speed result in focusing, and regions of increased effective sound speed result in defocusing (analogous to a divergent lens). Indeed, the formation of focusing regions and shadow areas due to random focusing and defocusing of the wave is clearly observed in Fig. 3. Regions of increased pressure follow, as expected, regions of minimum values of the velocity field. The maximum positive peak pressure $V = 2.6$ is reached in the case of nonlinear propagation, whereas $V = 1.5$ in the case of linear propagation. In spite of the additional absorption at the shocks, the maximum of peak positive pressure in the nonlinear case is higher than that in the linear case, even at distances of 60 wavelengths (three shock formation lengths).

The structure of the acoustic field (Figs. 3a and 3b) is formed mainly due to the presence of the longitudinal component $U_\parallel$ of the random velocity field. The transverse component acts as a flow randomly shifting the focusing and shadow zones perpendicularly to the direction of wave propagation. Note that, for the chosen characteristics of inhomogeneities (small size $L = 3\lambda$ and relatively low amplitude $M = \max(U_\parallel, U_\perp) = 0.03$), the inclusion of the random transverse velocity component in the computation did not noticeably affect the resulting structure of the acoustic field. However, the effect of the transverse velocity component becomes stronger when the scale (structure size) of inhomogeneities L increases, in particular, in the presence of a constant flow in the transverse direction. Let us consider, as an example, a combination of a random velocity field (Fig. 2) with a constant transverse flow $U_\perp^0 = 0.1$. The results of simulation of the corresponding nonlinear acoustic field ($N = 0.05$) are presented in Fig. 3c for the peak positive pressure. Note that, in this case, the flow shifts not only the acoustic field but also the random velocity inhomogeneities. Therefore, when the uniform

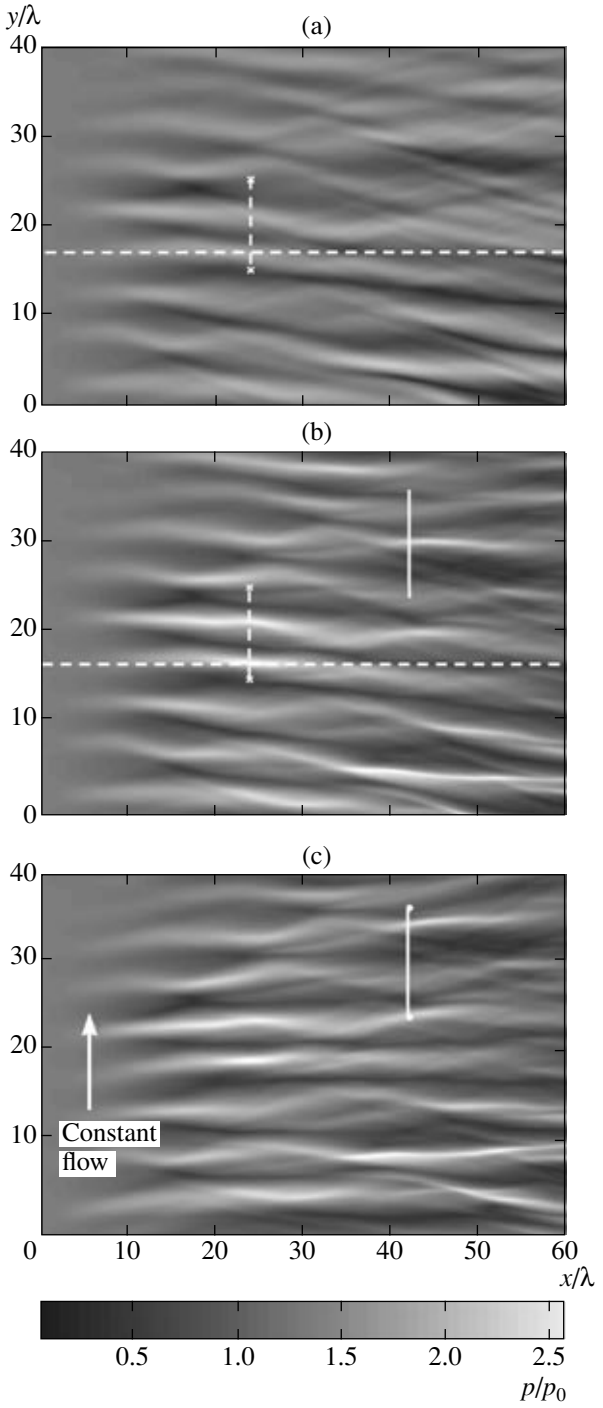

Fig. 3. Spatial patterns of the peak positive pressure corresponding to (a) linear ($N = 0$) and (b) nonlinear ($N = 0.05$) propagation of an initially plane harmonic wave through the randomly inhomogeneous moving medium. (c) The result for nonlinear propagation ($N = 0.05$) in the presence of an additional transverse constant flow $U_\perp^0 = 0.1$. The vertical solid line shows the position of the transverse field distribution presented in Fig. 4, the dashed vertical line, of the transverse distributions in Fig. 5, and the dashed horizontal line, of the longitudinal distributions in Fig. 6.

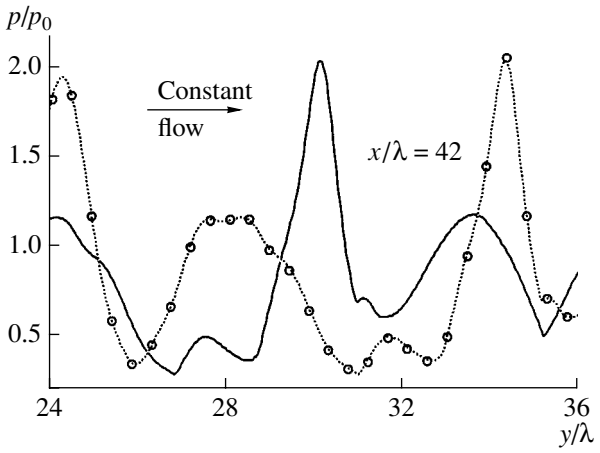

Fig. 4. Distributions of peak positive pressure along the transverse segments (solid lines) shown in Figs. 3b and 3c at the distance $x/\lambda = 42$. The solid curve refers to the propagation through random velocity field (Fig. 3b), the dotted curve, to the analytic transformation of the numerical solution to account for the additional constant flow, and the small circles, to the full numerical solution in the presence of the flow (Fig. 3c).

flow was superimposed on the random field velocity distributions, the random field was transformed to account for the spatial shift of the inhomogeneities in the transverse direction due to the presence of the flow. The resulting velocity field then was used in the simulations of the acoustic field. For this purpose, the constant velocity $U_\perp^0$ was introduced in Eq. (6). A noticeable shift of the field towards the direction of the flow without changing the morphology of the field is clearly observed. Note that the results for the acoustic field in the presence of constant flow, which are given in Fig. 3c, can also be obtained without additional simulations but using the numerical results for the case without the flow (however, with shifted random inhomogeneities) and analytic transformations (7) and (8), which eliminate the mean flow from parabolic equation (6).

To illustrate the effect of shifting the nonlinear acoustic field by the constant flow without changing its spatial structure, three one-dimensional transverse distributions are presented in Fig. 4. The positions of the distributions are denoted by the transverse solid lines shown in Figs. 3b and 3c at a distance of $x/\lambda = 42$. In Fig. 4, the solid curve is the peak positive pressure modeled with the presence of only random inhomogeneities, the dotted line is the result in the presence of inhomogeneities and a uniform flow based on the analytic transformation, and the circles show the purely numerical result in the presence of inhomogeneities and a uniform flow. It is seen that the transformation is in excellent agreement with the direct numerical results, which provides an additional verification of the algorithm used in modeling the transverse component of the velocity field.

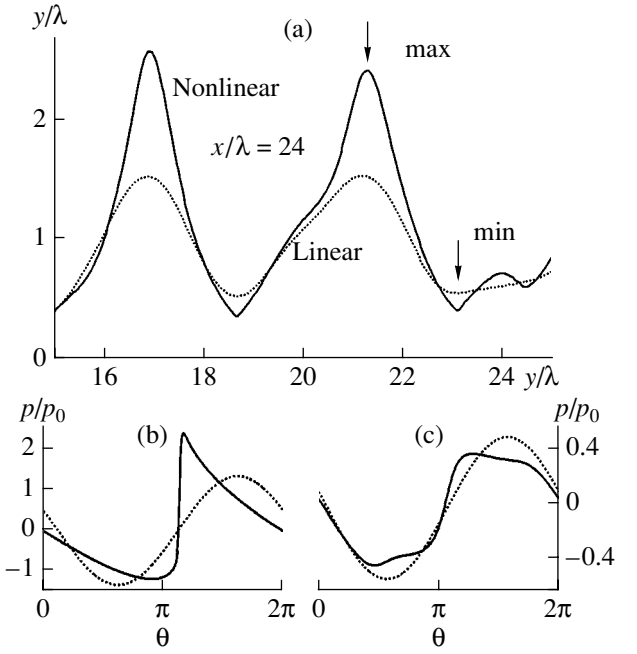

Fig. 5. (a) Transverse distributions of the peak positive pressure at the distance $x/\lambda = 24$ along the dashed segments shown in Fig. 3 for linear ($N = 0$, the dotted line) and nonlinear ($N = 0.05$, the solid line) propagation. (b) Linear and nonlinear waveforms at the points of maximum positive pressure $x/\lambda = 24$, $y/\lambda = 21.3$ (indicated as max in plot (a)). (c) Waveforms at the pressure minimum $x/\lambda = 24$, $y/\lambda = 23.15$ (indicated as min in plot (a)).

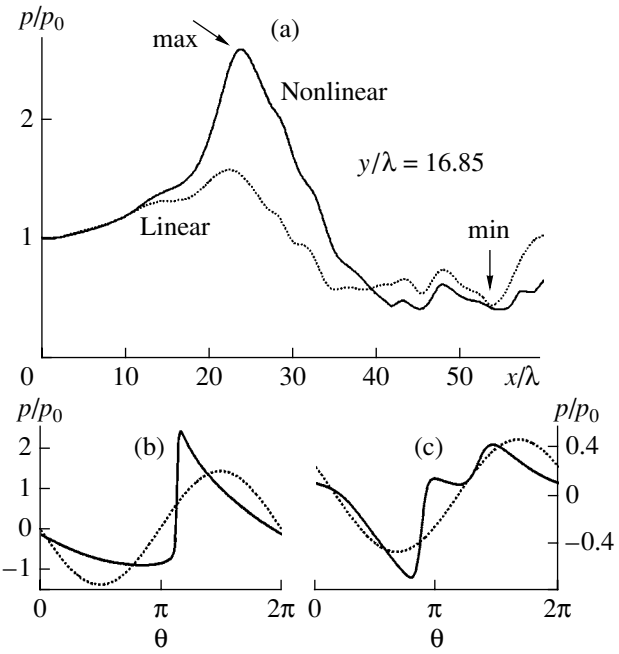

Fig. 6. (a) Longitudinal distributions of the peak positive pressure for linear ($N = 0$, the dotted line) and nonlinear ($N = 0.05$, the solid line) propagation along the dashed line $y/\lambda = 16.85$ shown in Fig. 3. (b) Linear and nonlinear waveforms at the points of maximum positive pressure $x/\lambda = 24$, $y/\lambda = 16.85$ (indicated as max in plot (a)). (c) Waveforms at the pressure minimum $x/\lambda = 54$, $y/\lambda = 16.85$ (indicated as min in plot (a)).

To illustrate the effect of acoustic nonlinearity on the wave propagation in a randomly inhomogeneous medium, two one-dimensional distributions of peak positive pressure across and along the traveling x coordinate are presented in Figs. 5 and 6. The solutions correspond to linear ($N = 0$, dotted curves) and nonlinear ($N = 0.05$, solid curves) propagation within the dashed line intervals shown in Figs. 3a and 3b. It is seen that nonlinearity results in much higher peak pressures in focal regions, narrowing of the increased pressure area, and a shift of the maximum peak pressure in both the longitudinal and transverse directions. Even at ranges of three shock formation distances, despite the existence of strong nonlinear dissipation at the shocks, regions of increased pressure level are observed due to the transverse redistribution of acoustic energy (see Fig. 3). Linear and nonlinear waveforms that correspond to positions of the maximum and minimum in the peak pressure distributions are also shown in Figs. 5 and 6. In the focal regions (Figs. 5b and 6b), typical asymmetric distortion of the waveform with a developed shock front, an increased positive peak, and a smoothed negative part of the waveform was observed in the case of nonlinear propagation. In regions of pressure minima, the nonlinear waveforms (Figs. 5c and 6c) still demonstrated significant distortion, but, in this case, shocks were absent, presumably because the higher harmonic components were due to scattering from the focused regions.

The effective absorption of acoustic energy, with and without the presence of random inhomogeneities, can be compared by using the propagation curves for normalized intensity averaged over the transverse coordinate at every step in propagation distance x. Figure 7 shows the results for linear propagation in either homogeneous or inhomogeneous absorptive medium (the upper solid curve), for nonlinear propagation in a homogeneous medium using weak shock theory (WST; the upper dotted curve) and with absorption explicitly modeled (the Burgers equation; the lower dotted curve), and for nonlinear propagation in a randomly inhomogeneous medium (the nonlinear parabolic equation (NPE); the lower solid curve). Some energy dissipation (~20% at a distance of 60 wavelengths) in the case of linear propagation is due to the inclusion of the same absorption ($A = 0.002$) as that used in the nonlinear simulations. The Burgers and NPE nonlinear simulations show similar energy loss as the linear code for distances up to one shock formation distance (about 20 wavelengths for $N = 0.05$). Beyond this range, the main contribution to the energy loss (~60–70%) is due to strong nonlinear absorption at the shocks. Note that the energy dissipation in a nonlinear homogeneous medium (Burgers equation) is almost the same as in a

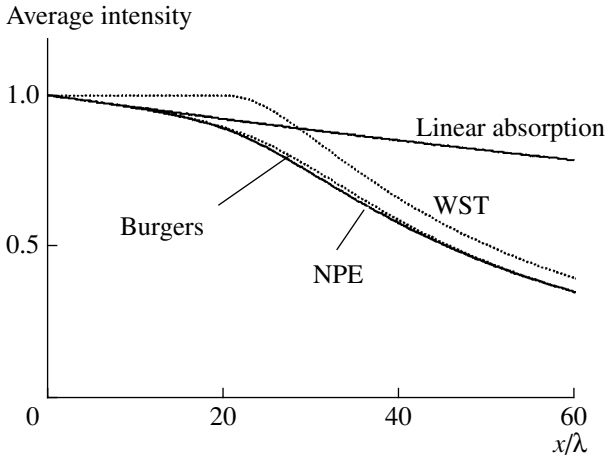

Fig. 7. Propagation curves for the wave intensity averaged over the transverse coordinate: linear propagation in a dissipative medium, nonlinear propagation governed by the weak shock theory (WST), nonlinear plane wave propagation in a dissipative medium (Burgers equation), and nonlinear propagation in a moving inhomogeneous dissipative medium governed by the nonlinear parabolic equation (NPE). Parameters of simulations are $N = 0.05$, $A = 0.002$, and $N_{max} = 150$.

nonlinear inhomogeneous medium (NPE). A small difference could be seen only at distances from one to two shock formation lengths (20–40 wavelengths). The presence of inhomogeneities thus does not lead to noticeable changes in energy losses. The use of the weak shock theory does not model the energy losses at small distances, and, at long ranges, its results appear to be offset by an amount similar to the linear losses.

5. CONCLUSIONS

Thus, a new parabolic equation for the propagation of nonlinear sound in inhomogeneous moving media was presented in this paper. The equation is an extension of the KZK equation for nonlinear beams generalized for arbitrary inhomogeneous media. In particular, we have taken into account the component of motion of the medium in the direction perpendicular to the wave propagation direction. The assumptions invoked in deriving this generalized equation were that the fluctuations in the properties of the medium varied slowly in space and in time and that the fluctuations of the speed of sound and velocity of the medium were small in magnitude as compared to the speed of sound. The diffraction is modeled using the parabolic approximation, which restricts the validity of the solution to collimated beams and is generally accepted to be a good model for sound with propagation direction within 20° about the axis. Therefore, this model is appropriate for considering the inhomogeneities that primarily result in scattering in the forward direction.

A numerical algorithm, which allows the investigation of a wide number of problems of intense periodic wave propagation through different types of inhomogeneities, was developed. The derived parabolic equation was found to have properties of similarity, which makes it possible to find solutions for certain types of mean motion of the medium in the presence of small fluctuations by using the solution for effective fluctuations. These properties were used to verify the accuracy of the numerical algorithm and to study the effect of lateral flow on the structure of the acoustic field. It was shown that, when a nonfluctuating flow component was included, the acoustic field was shifted by convection but still retained the same morphology (focal regions and shadow zones) as that predicted for the case without the transverse flow component.

The propagation of an initially harmonic plane wave in a nonlinear moving medium was investigated for a single realization of a random field with two-dimensional inhomogeneities. The simulations showed that the acoustic field was primarily affected by the fluctuations in the sound speed or flow component parallel to the wave propagation direction. The transverse component of the random flow was negligible for small-scale inhomogeneities. We considered other realizations with different length scales, and the interpretations presented here remain valid with the exception that, for inhomogeneities with length scales much longer than the acoustic wavelength, the impact of the transverse velocity field becomes noticeable.

It was shown that, for the case where nonlinearity has a length scale on the order of the caustic formation length, the focusing of the wave was enhanced even in the presence of nonlinear dissipation; that is, the focal regions have higher peak pressure and are more localized. In the focal regions, the waveforms were classical in shape with shock fronts, cusped positive peaks, and smooth negative troughs. In the shadow zones, the presence of nonlinearity could also be observed, since the waveforms were not sinusoidal but had significant harmonic content. However, the waveforms did not exhibit shock fronts, indicating that the phases of the harmonics were not aligned, presumably due to multipath propagation in the medium. The presence of nonlinearity, therefore, was most noticeable in the focal regions but also affected the waveforms in the shadow zones. The energy of the acoustic wave that propagated through the inhomogeneous medium was very close to that predicted by the plane wave theory. Hence, the transverse redistribution of energy into higher (with extra absorption) and lower (with less absorption) pressure regions did not on the average result in any significant change in nonlinear energy losses.

ACKNOWLEDGMENTS

We are grateful to V. E. Ostashev and O. A. Godin for helpful discussions. This work was supported by the Russian Foundation for Basic Research and the INTAS, NATO, and CNRS grants.

REFERENCES

1. V. I. Tatarski, *The Effects of Turbulent Atmosphere on Wave Propagation* (Nauka, Moscow, 1967; IPTS Keter Press, Jerusalem, 1971).
2. V. E. Ostashev, *Acoustics in Moving Inhomogeneous Media* (E&Fn Spon, London, 1997).
3. *Ocean Acoustics*, Ed. by L. M. Brekhovskikh (Nauka, Moscow, 1974) [in Russian].
4. O. A. Godin, Dokl. Akad. Nauk SSSR **293** (1), 63 (1987).
5. *Physical Principles of Medical Ultrasonics*, Ed. by C. R. Hill (Ellis Horwood, Chichester, 1986; Mir, Moscow, 1989).
6. O. A. Godin, J. Acoust. Soc. Am. **112**, 1269 (2002).
7. O. V. Rudenko, A. K. Sukhorukova, and A. P. Sukhorukov, Akust. Zh. **40**, 290 (1994) [Acoust. Phys. **40**, 264 (1994)].
8. O. V. Rudenko, A. K. Sukhorukova, and A. P. Sukhorukov, Akust. Zh. **43**, 396 (1997) [Acoust. Phys. **43**, 339 (1997)].
9. V. E. Ostashev, D. Juve, and Ph. Blanc-Benon, Acta Acust. Acust. **83**, 455 (1997).
10. L. Dallois, Ph. Blanc-Benon, and D. Juve, J. Comput. Acoust. **9**, 477 (2001).
11. O. A. Godin, Dokl. Phys. **47**, 643 (2002).
12. Ph. Blanc-Benon, B. Lipkens, L. Dallois, et al., J. Acoust. Soc. Am. **111**, 487 (2002).
13. B. E. McDonald and W. A. Kuperman, J. Acoust. Soc. Am. **81**, 1406 (1987).
14. E. N. Pelinovskiĭ, V. E. Fridman, and Yu. K. Engel'brekht, *Nonlinear Equations of Evolution* (Valgus, Tallinn, 1984).
15. V. A. Khokhlova, P. Blanc-Benon, M. V. Averiyanov, and R. O. Cleveland, in *Proceedings of the 2004 IEEE UFFC, 2004*, pp. 533–536.
16. O. V. Rudenko and S. I. Soluyan, *Theoretical Foundations of Nonlinear Acoustics* (Nauka, Moscow, 1975; Plenum, New York, 1977).
17. R. O. Cleveland, J. P. Chambers, R. Raspet, et al., J. Acoust. Soc. Am. **100**, 3017 (1996).
18. V. A. Khokhlova, R. Souchon, J. Tavakkoli, et al., J. Acoust. Soc. Am. **110**, 95 (2001).
19. W. H. Press, S. A. Teukolsky, W. T. Vetterling, and B. P. Flannery, *Numerical Recipes in FORTRAN* (Cambridge Univ. Press, New York, 1992).
20. M. Karweit, Ph. Blanc-Benon, D. Juvé, and G. Comte-Bellot, J. Acoust. Soc. Am. **81**, 52 (1991).